ARTICLE

Unique Lithiation and Delithiation Processes of Nanostructured Metal Silicides

Sa Zhou and Dunwei Wang*

Department of Chemistry, Merkert Chemistry Center, Boston College, 2609 Beacon Street, Chestnut Hill, Massachusetts 02467, United States

ABSTRACT We report that $TiSi_2$ nanonet exhibits considerable activities in the reversible lithiation and delithiation processes, although bulk-sized titanium silicide is known to be inactive when used as an electrode material for lithium ion batteries. The detailed mechanism of this unique process was studied using electrochemical techniques including the electrochemical impedance spectroscopy (EIS) method. By systematic characterizations of the Nyquist plots and comparisons with the microstructure examinations, we identified the main reason for the activities as the layered crystal structure that is found stable only in $TiSi_2$ nanonets. The layer structure is characterized by the existence of a Si-only layer, which exhibits reactivity when exposed to lithium ions. Control studies where $TiSi_2$ nanowires and $TiSi_2$/Si heteronanostructures were involved, respectively, were performed. Similar to bulk $TiSi_2$, $TiSi_2$ nanowires show limited reactivity in lithium ion insertion and deinsertion; the EIS characteristics of $TiSi_2$/Si heteronanostructures, on the other hand, are distinctly different from those of $TiSi_2$ nanonets. The result supports our proposed $TiSi_2$ nanonet lithiation mechanism. This discovery highlights the uniqueness of nanoscale materials and will likely broaden the spectrum of electrode material choices for electrochemical energy storage.

KEYWORDS: titanium silicide · nanonets · lithium ion battery · anode · electrochemical impedance spectroscopy

Modern technological developments create a daunting demand for portable electrical energy storage devices with ever higher energy density and power density. As a relatively recent invention, Li ion battery stands out among the available approaches to meeting this demand for its lightweight, long lifetime, and good cycleability. Despite enormous efforts, the progress of Li ion battery research has lagged behind significantly when compared with many other areas such as personal electronics, thanks to the rapid growth of the demand, and has become a weak link in the technological developments. One key hurdle in advancing Li ion battery performance is the limited availability of materials.[1] The magnitude of difficulties in finding a suitable candidate may be appreciated by examining what constitutes an "ideal" anode electrode. The chosen material needs to meet a number of intrinsic property requirements simultaneously, including being low density to be lightweight; possessing the right chemical reactivity to permit reversible Li ion insertion and extraction for good cycleability; the Li ion insertion and extraction reactions are desired to occur at low potentials compared with the reactions taking place at the cathode to afford high cell potentials; the reactions also need to proceed in a controllable fashion so that no unmanageable heat is generated.[2] The complexity of these requirements greatly limits our choices of candidates when selecting electrode materials.

To meet this challenge, considerable attention has been paid to studying novel morphologies of existing compounds, particularly those in the nanoscale.[3−12] For example, phase transitions permitted only by nanoscale materials have been demonstrated to be beneficial for high power density.[13,14] The high surface area of nanomaterials has also been identified to lead to electrode capacities significantly higher than what is "theoretically" possible for bulk materials.[15] These new phenomena associated with the small dimensions of nanomaterials compel us to expand the efforts of studying nanostructures as potential electrode materials for Li ion batteries. In line with these observations, we report high reactivities in nanoscale metal silicides, $TiSi_2$ nanonets, although the bulk counterpart of this composition has been deemed inactive when exposed to similar electrolyte systems.

We are drawn to study metal silicides because of their high electrical conductivities, which has been exploited to complement C or Si to boost their performance as electrode materials.[8,16−23] Similarly, when $TiSi_2$

*Address correspondence to dunwei.wang@bc.edu.

Received for review August 28, 2010 and accepted September 30, 2010.

Published online October 13, 2010. 10.1021/nn102194w

nanonets, a unique two-dimensional nanostructure discovered by us,[24,25] are interfaced with Si nanoparticles, the resulting materials show significantly improved cycleability and power density.[26] While low dimensional metal silicides with morphologies similar to $TiSi_2$ nanonets (albeit simpler, *e.g.*, nanowires) have been widely studied for electronic applications, studies of these materials for electrochemical energy storage have not been encountered. The underwhelming interest may be in part due to the previously reported low activities of their bulk crystals.[17] Our results presented here reveal that the properties of $TiSi_2$ nanonets differ from bulk $TiSi_2$ drastically. The layered crystal structure of C49, which is only stable in the nanonet form, is the primary reason for the activities.[24] With the detailed mechanism of the lithiation process unraveled, the results are likely to stimulate interest in low dimensional metal silicide nanostructures and discover new properties that are beneficial to the rapidly developing energy materials research field.

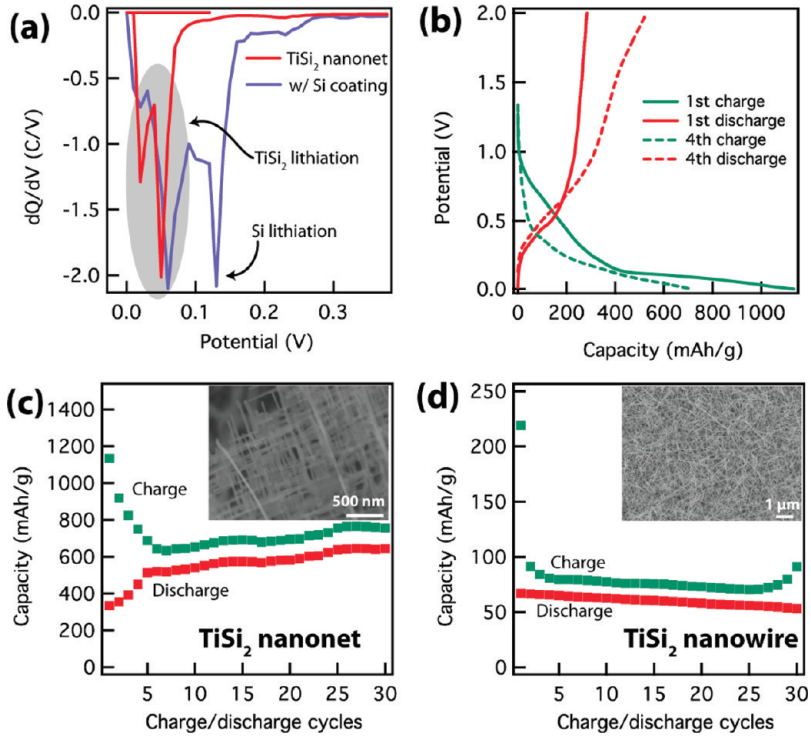

Figure 1. The unusual reactivity of $TiSi_2$ nanonets. (a) The shaded peaks in the EPS data (for clarity, only the portion that corresponds to charge is shown) are due to the lithiation processes. For comparison, the EPS data of $TiSi_2$/Si heteronanostructures are also shown (labeled w/Si coating). (b) The charge/discharge behaviors (data from the 1st and 4th charge/discharge cycles as shown in panel c) confirm the reactivity of $TiSi_2$ nanonets and provide a quantitative measure of the capacity, which is substantial considering that bulk $TiSi_2$ is inactive (charge rate: 1000 mA/g, equvalent to C/2 if we assume all Si atoms in $TiSi_2$ participate in the lithiation process). (c) The reactivity is maintained for at least 30 cycles with negligible capacity fading. (d) Much lower charge/discharge capacity is measured when $TiSi_2$ nanowires are tested. $TiSi_2$ nanowires have similar sizes to but have different crystal structures from $TiSi_2$ nanonets.

RESULTS AND DISCUSSIONS

The reactivity of $TiSi_2$ nanonets with Li ions (Li^+) is evidenced by the peaks between 0 and 0.09 V in the EPS data (Figure 1a). This conclusion is also supported by the charge/discharge characteristics as shown in Figure 1b. Although various metal silicides have been studied in the past, they mostly act as the inactive component in the composites because their reactivity with Li^+ has been found to be too low to be exploited with a few exceptions including Mg_2Si and $NiSi_2$.[17] With this background information in mind, we were surprised by the observed lithiation peaks in the EPS data and the unequivocal evidence of the high charge capacity (>600 mAh/g) and discharge capacity (>500 mAh/g). Furthermore, the material survives repeated charge/discharge treatments for at least 30 cycles with the capacity maintained above 500 mAh/g. During the first four cycles, the discharge capacity increased rapidly from 334 mAh/g (1st cycle, with a 30% Coulombic efficiency) to 512 mAh/g (5th cycle, Coulombic efficiency of 75%); afterward, the discharge capacity steadily increased to 600 mAh/g (21st cycle) with a relatively stable Coulombic efficiency of ~85% (Figure 1c). We note that these values do not represent the best performance that can be achieved on $TiSi_2$ nanonets because the experimental parameters for the charge/discharge characterizations are not yet optimized. Although lower than Si and several transition metal oxides, this value is higher than commercially used graphite. Combined with the low reaction potentials (0.1−0.5 V), this result is significant in itself. Nevertheless, we emphasize that the focus of this report is on understanding the mechanism of the lithiation and delithiation processes.

The unusual crystal structure of $TiSi_2$ nanonet plays an important role in this unexpected phenomenon. Our previous study reveals that two-dimensional $TiSi_2$ nanonets assume a crystal structure known as C49, an unstable phase for bulk $TiSi_2$.[24] This structure is characterized by an orthorhombic unit cell where a Si-only layer appears every few atomic layers of mixed Ti and Si (the adjacent Si-only layers are separated by approximately 10.32 Å).[27] Indeed, this Si-only layer covers the surface of $TiSi_2$ and acts as the driving force for the formation of the nanonet morphology. Owing to its well-known reactivity with Li^+, the Si layers serve as the host for the Li^+ insertion. A competing explanation may be found in the small sizes, which has been predicted to induce lithiation for materials that show no reactivity at bulk sizes.[3] This possibility is ruled out because $TiSi_2$ nanowires of C54 crystal structure (a stable phase shared by bulk $TiSi_2$ crystals) exhibit low charge or discharge capacity (<100 mAh/g), Figure 1d. Nonetheless, since the existence of the stable C49 is only observed

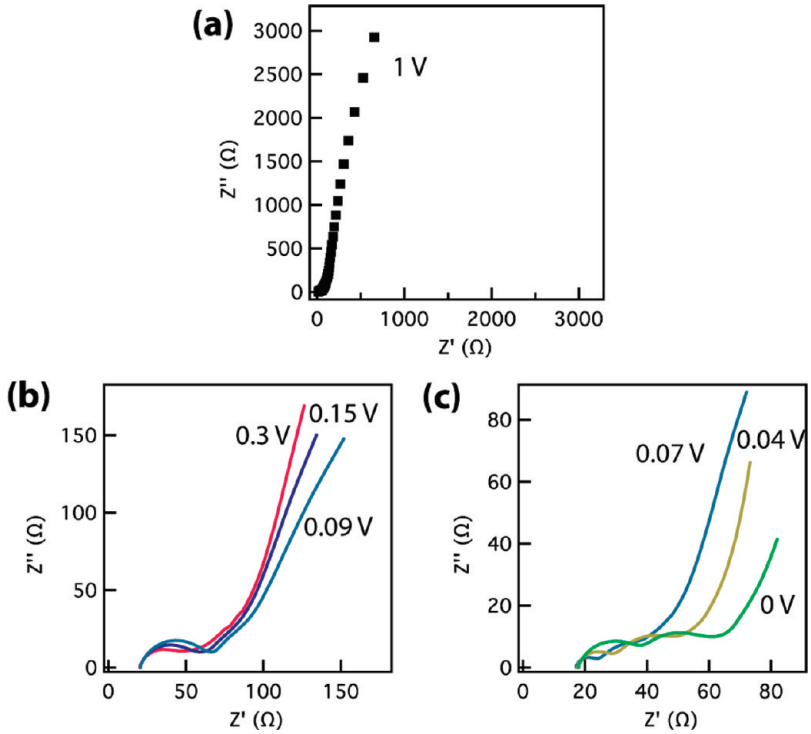

Figure 2. Nyquist plots of $TiSi_2$ nanonets under different charge conditions: (a) 1, (b) 0.3−0.09, (c) 0.07−0 V. For clarity, the data are plotted as lines in panels b and c.

in $TiSi_2$ nanonets, the reactivity is unique to the nanoscale sizes.

Although the reactivity originates from the existence of Si in $TiSi_2$ nanonets, the property is distinctly different from crystalline Si. The peak positions (0−0.09 V), for instance, are more negative than what is expected from Si. As a comparison, the EPS data of $TiSi_2$ nanonets with intential Si coating are plotted in Figure 1a. The lithiation peak position (approximately 0.13 V) agrees with literature reports on Si of other forms (bulk crystal, thin films, or nanowires). This difference indicates that the detailed lithiation process of $TiSi_2$ nanonets is unique and deserves more attention. Using the EPS data as a guideline, we next compare the results of the EIS studies of $TiSi_2$ at different charge/discharge potentials. The potentials at which the EIS measurements were performed were chosen to allow us to examine $TiSi_2$ before (*e.g.*, at 1 and 0.3 V), during (*e.g.*, at 0.15−0.04 V) and after lithiation (*e.g.*, at 0 V). In a similar fashion, the EIS characterizations aimed at understanding the delithiation processes were carried before and after the delithiation. EIS studies of $TiSi_2$/Si heteronanostructures were conducted following the same principle. The availability of the EPS data was the key enabling factor to permit us to choose the potentials in a meaningful way.

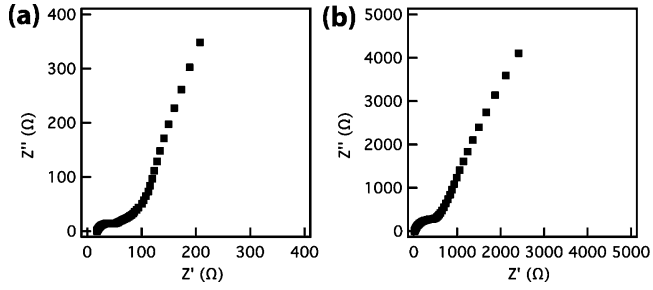

Figure 3. The Nyquist plots of $TiSi_2$ nanonets at different stages of the discharge process: (a) 0.4 and (b) 1 V. Note the differences of the scales in these two plots. The semicircle due to the reactions during the charge process persists, as is evidenced in panel b.

As a powerful electrochemical technique, EIS provides critical information on the electrodes, the electrolyte and the electrode/electrolyte interface under steady-state conditions and has been widely utilized.[28−36] To understand the unique lithiation process of the $TiSi_2$ nanonets, we chose to create the Nyquist plots under different applied potentials, 1, 0.3, 0.15, 0.09, 0.07, 0.04, and 0 V for the charge cycle and 0.4 and 1 V for the discharge cycle. The data are presented in Figure 2 and Figure 3. Several features of this group of data are worth emphasizing: (i) The evolution of the semicircle arcs is obvious. The semicircle in the high frequency range carries information on the characteristics of the solid electrolyte interface (SEI).[28,34] It appears shortly after the equilibrium of the system is established. (ii) At 0.09 V, the semicircle associated with the SEI is fully developed, and a new semicircle toward the lower frequency region starts to take form. Important to the understanding of this newly formed semicircle is that the lithiation peaks in the EPS data emerge below 0.09 V (Figure 1a). We therefore suggest that the appearance of this semicircle is associated with the solid-state reactions due to the lithiation process. (iii) The second semicircle is fully developed when the $TiSi_2$ nanonets are fully charged (at 0 V). (iv) The real part of the impedance at the high frequency end is consistent, approximately 20 Ω for all applied potentials. This value quantifies the series resistance of the system, including the resistance of the electrolyte and that of the contact. (v) Upon discharge, the second semicircle (due to the lithiation process) persists while the first one (associated with the SEI) disappears. The origin of this seemingly paradoxical feature will be discussed later in this article. (vi) Lastly, upon discharge the impedance returns to a level similar to the initial state.

On the basis of this observation, we postulate the following $TiSi_2$ nanonet lithiation mechanism. When a relatively high potential is applied to the $TiSi_2$ nanonets (*e.g.*, >0.3 V), no lithiation takes place; the potential drop mainly occurs in the solution and at the SEI, which is characterized by low impedance at high frequencies and high impedance at low frequencies (*i.e.*, capacitive features).[28,34] As the applied potentials are decreased to the point where the lithiation process

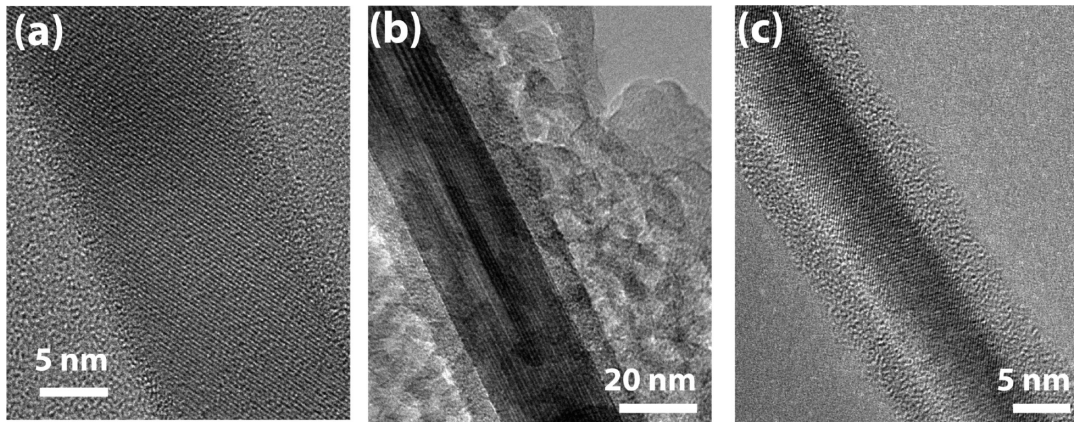

Figure 4. TEM data of $TiSi_2$ nanonets before lithiation (a) and after lithiation (b), and after delithiation (c).

starts to occur (<0.09 V), a second interface in addition to the SEI takes form, which corresponds to the appearance of the second semicircle. The origin of this second interface comes from the reaction between Li^+ and $TiSi_2$, which enriches Si to the surface because there are no known chemical reactions between Ti and Li^+. During the delithiation process, this interface persists because the enriched Si on the surface of $TiSi_2$ remains.

This hypothesis is supported by the microstructure studies. Figure 4 shows a $TiSi_2$ nanonet before the lithiation, after the lithiation, and after the delithiation. We see that the lithiation process produces a layer of amorphous coating on the surface of $TiSi_2$, which contains significantly higher concentration of Si than that of Ti (Si:Ti ≈ 50:1) as identified by EDX characterizations. Owing to the instrumentation limitation, we could not quantify the amount of Li in this amorphous layer. The crystalline nature of the $TiSi_2$, where the Si:Ti ratio is maintained at 2:1, is preserved. This finding is important because the existence of a charge transporter is essential to the high power density and the good cycleability. The result suggests that the lithiation process proceeds by selective enrichment of Si on the surface of $TiSi_2$. The second semicircle in the Nyquist plot toward the end of the charge process can be attributed to the interface between this amorphous layer and crystalline $TiSi_2$. We suggest that the excess Ti as a result of the Si extraction from $TiSi_2$ dissolves in the electrolyte solution. Occasionally we observed crystallites of Ti in the amorphous layer, but this observation is not consistent, probably due to the instability of the Ti crystallites. After delithiation, this amorphous layer maintains its form. This observation is consistent with the fact that the semicircle that appeared during the lithiation process persists after delithiation. It supports our hypothesis that the second semicircle may be ascribed to the interface between the enriched Si and $TiSi_2$.

SEM characterizations reveal information consistent with the TEM data. When the applied potentials are high (>0.15 V), the $TiSi_2$ nanonets appear intact, and the branches are distinguishable. Starting at 0.09 V, a layer of coating becomes obvious on the surface of the

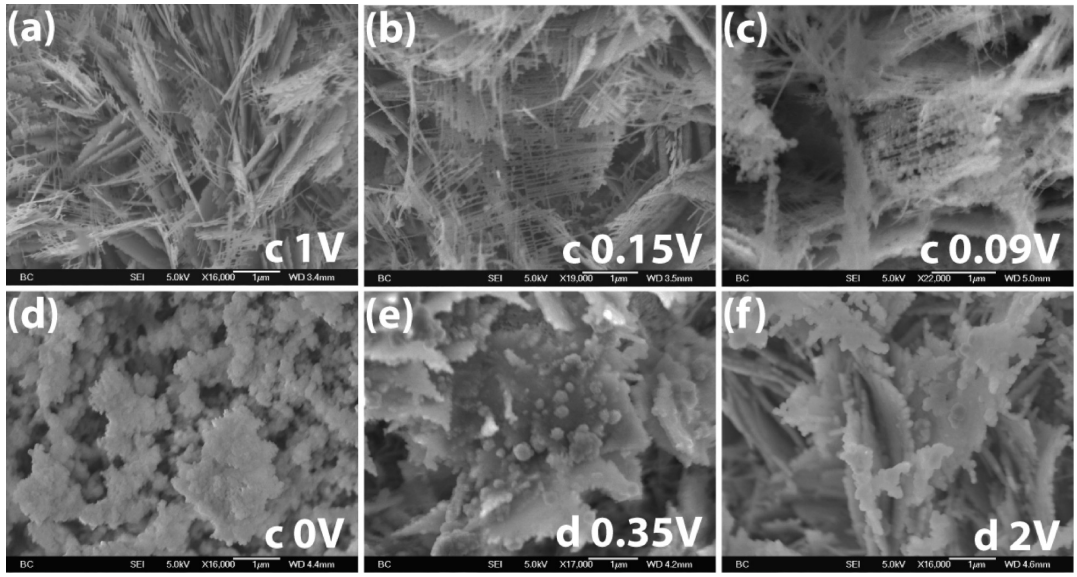

Figure 5. SEM data of $TiSi_2$ nanonets at different stages of the lithiation (a−d) and the delithiation processes (e and f). Scale bars in all figures: 1 μm.

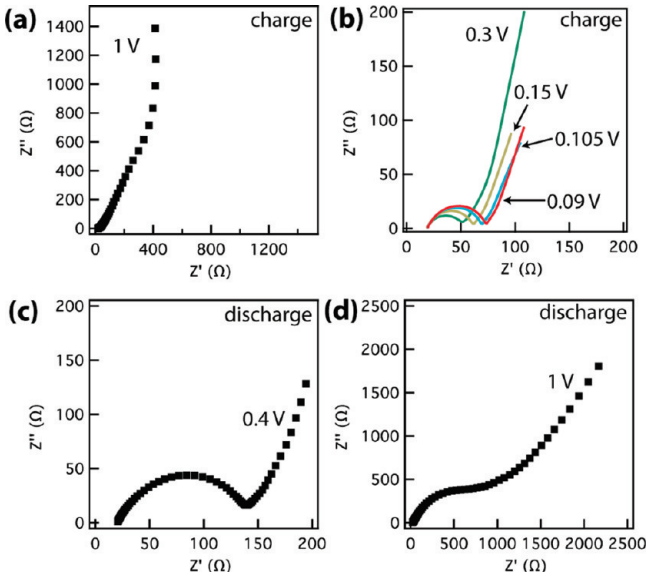

Figure 6. The Nyquist plots of $TiSi_2$/Si heteronanostructures at different stages of charge/discharge.

nanonets, which intensifies as the potential is further dropped until the charge process is complete (at 0 V). Upon delithiation, the coating persists and the network characteristic of $TiSi_2$ is no longer distinguishable. Under SEM, the branches appear to melt together, and each nanonet looks like a flake.

Although the lithiation process of $TiSi_2$ takes place by reactions between Si and Li^+, the characteristics are different from that of Si of other forms. To demonstrate this difference, we next examine the EIS data of $TiSi_2$ nanonets with intentional Si coating (*i.e.*, $TiSi_2$/Si heteronanostructures), Figure 6. While the general trend agrees with that in Figure 2, only one semicircle is observed in the Nyquist plots for the $TiSi_2$/Si heteronanostructures, suggesting that the capacitive impedance of the $TiSi_2$/Si interface in the heteronanostructure is insignficant. This finding is consistent with our previous observations[26] and underlines the advantage of having the $TiSi_2$ nanonet in the heteronanostructure design: charges transfer from Si to $TiSi_2$ without significant resistance to allow for high power density. The fact that the second semicircle only appears in the data measured on $TiSi_2$ nanonet samples indicates that the interface between the $TiSi_2$ and the enriched Si is defective, more so than the interface between the $TiSi_2$ and the deposited Si. The result exemplifies the importance of obtaining a high-quality interface when making heteronanostructures. Nonetheless, it is worth noting that to preserve $TiSi_2$ when testing the heteronanostructures we limited the charge potentials to be above 0.09 V. When the charge potentials were pushed below this limit, reactions between Li^+ and $TiSi_2$ nanonets dominated.

Quantitative information on the $TiSi_2$ nanonet lithiation processes may be extracted from the Nyquist plots by fitting the data using the equivalent electrical circuits (EEC) method.[28] To perform this function, we used the EECs as shown in Figure 7, where CPE stands for constant phase elements. The usage of CPE rather than capacitors accounts for the imperfections of the Helmoholtz double layer due to, for example, the nanoscopic nature of the electrode surfaces. In calculating the Nyquist plot for the $TiSi_2$/Si heteronanostructures, we employed two $R//Q$ elements. $R_1//Q_1$ is used to simulate the SEI and the charge transfer process;[30,32,33,35] and $R_d//Q_d$ is used to simulate the diffusion process.[29,34] The calculated Nyquist plot overlaps with the measured one well, with an error of 1.12×10^{-4} (which is the χ^2 value between the fitting and the experimental data as generated by the simulation software, Zsimpwin). On the basis of the EEC and the excellent agree-

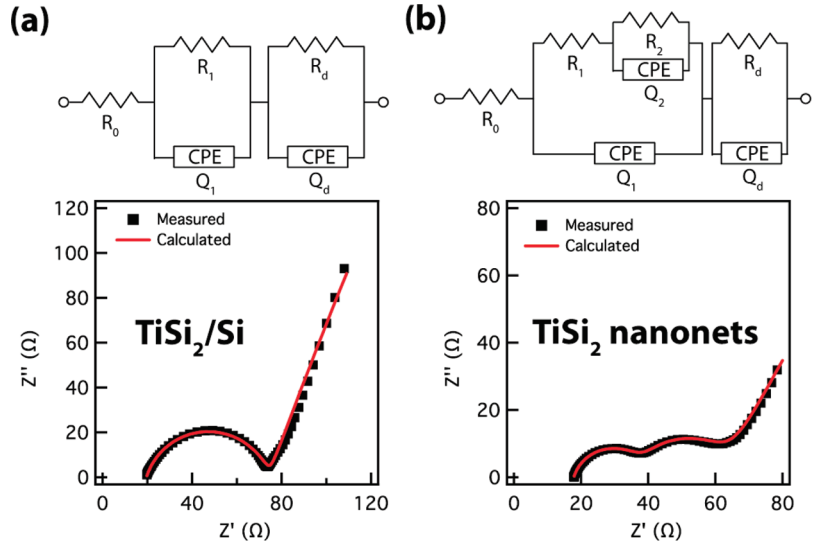

Figure 7. Understanding the Nyquist plot using equivalent electrical circuits for (a) $TiSi_2$/Si heteronanostructures and (b) $TiSi_2$ nanonets. (Top panels) The equivalent electrical circuit; (bottom panels) the comparison of the measured data and the calculated data (at 0.09 V for $TiSi_2$/Si and 0 V for $TiSi_2$nanonets, respectively). The meanings of the labels are discussed in the main text.

ment between the calculated data and the measured data, we understand that the semicircle in the Nyquist plot can be ascribed to the processes at the SEI and the charge transfer. The increase of the impedance at the low frequency end following a nearly linear relation is due to the diffusion of Li^+ in the electrolyte. This understanding is consistent with the literature reports on other forms of Si and agrees well with our hypothesis as discussed earlier.

To fit the Nyquist plot of the $TiSi_2$ nanonet, we introduced an additional $R//Q$ element ($R_2//Q_2$) to account for the processes taking place at the interface of $TiSi_2$ and the enriched Si. With this element added, we achieved an excellent agreement between the calculated data and the measured data (error: 9.59×10^{-5}); without this additional element, no sensible simulation was obtained. The result implies that the enriched Si differs from the deposited Si. We suggest that the difference orginates from the chemical reactions that dissociate Ti and Si in $TiSi_2$. More research is needed to fully understand the nature of this reaction.

The calculations also enabled us to obtain the quantitative values of the various resistive elements (*e.g.*, R_1 and R_2). Consider the data of the $TiSi_2$ nanonets. At different charge potentials, R_2 remains relatively constant, approximately 30 Ω. As discussed above, R_2 represents the resistance between the $TiSi_2$ and the enriched Si; once the interface is formed, its resistance is independent of the applied potentials. By contrast, R_1 increases from 24 Ω at 0.3 V to 47 Ω at 0.09 V charge potentials because of the SEI formation and its continued growth. This result further supports our hypothesis of the lithiation mechanism of the $TiSi_2$ nanonets.

CONCLUSIONS

New materials and new chemistry hold great promise for breakthroughs in the quest for high-density portable electrical power that can be stored and released at a fast rate. Finding new compounds or new forms of existing compounds are equally important parallel approaches that are actively pursued. For the latter, we have shown that $TiSi_2$ nanonets, a unique morphology that stabilizes C49 $TiSi_2$, exhibit unusually high activity compared with bulk titanium silicides. A specific capacity greater than 500 mAh/g is measured, and the material shows no obvious fading after 30 charge/discharge cycles. Through systematic electrochemical studies, we identified that the lithiation and the delithiation processes are enabled by the existence of Si-only atomic layers in $TiSi_2$ nanonets. The result highlights the exciting prospect of discovering new phenomenon in novel morphologies of existing materials.

EXPERIMENTAL SECTION

Following the protocols detailed in our previous reports,[24,25] we carried out the synthesis of $TiSi_2$ nanonets in a chemical vapor deposition (CVD) system. Briefly, a Ti foil (Sigma, 0.127 mm thick, purity: 99.7%) was used as the receiving substrate. The reaction chamber was heated to 675 °C. Then 50 sccm (standard cubic centimeter per minute) SiH_4 (10% in He, Voltaix), 100 sccm H_2, and 2.5 sccm $TiCl_4$ were delivered into the reaction chamber in tandem (P_{total}: 5 Torr). The reaction lasted 15 min, after which SiH_4 and $TiCl_4$ were stopped and the temperature was decreased to room temperature while H_2 flow was maintained to avoid oxidizing the resulting nanostructures. The system was pumped to its base pressure (<0.4 Torr) during the cooling process. The density of the resulting $TiSi_2$ nanonets was approximately 0.2 mg/cm^2. For comparison purposes, we also fabricated $TiSi_2$ nanowires and $TiSi_2$/Si heteronanostructures. The nanowire synthesis was similar to that of the nanonets except for the ratio of SiH_4 to $TiCl_4$; the details are reported elsewhere.[25] For the heteronanostructure synthesis, the temperature was brought to 650 °C after the growth of $TiSi_2$ nanonets; 80 sccm SiH_4 (10% in He) and 100 sccm H_2 were flowed at 15 Torr for 12 min to produce Si nanoparticles on the surface of $TiSi_2$ nanonets.

After growth, the sample was transferred to an Ar-filled glovebox (oxygen level < 2 ppm). Li ribbons were used as the counter and the reference electrodes, respectively. Separated by a polypropylene membrane (25 μm thick, Celgard 2500), the three electrodes ($TiSi_2$ or $TiSi_2$/Si on Ti foil and two Li ribbons) were rolled together and then immersed in the electrolyte (1.0 M $LiPF_6$ in 1:1 wt/wt ethylene carbonate and diethyl carbonate, Novolyte Technologies). Afterward, the device was placed in a sealed box within the glovebox to minimize the influences due to environmental fluctuations. The electrochemical measurements were conducted on a CHI 600C instrument.

The electrochemical potential spectroscopy (EPS) data were obtained by applying a series of potentials at 10 mV intervals to the working electrode.[37] At each step after the current decayed to 200 mA/g, the charges (Q) were calculated by integrating current over time. The electrochemical impedance spectroscopy (EIS) measurements were conducted at different charge/discharge states of $TiSi_2$ nanonets, $TiSi_2$ nanowires, and $TiSi_2$/Si heteronanostructures, respectively. The charge/discharge rate was set at 100 mA/g. The cell was allowed to reach equilibrium for 2 h before the impedance measurements. The frequency was varied between 50 kHz and 0.1 Hz, and the AC amplitude was 10 mV. All simulations were performed using ZsimpWin.

The samples before and after the lithiation and delithiation processes were imaged using a transmission electron microscope (TEM, model JEOL 2010F) and a scanning electron microscope (SEM, model JSM 6340). The TEM was operated at an accelaration voltage of 200 keV, and the SEM was working at 5 keV. Elemental analysis was conducted using an energy dispersive spectroscopy (EDS) attachment to the TEM.

Acknowledgment. We thank Boston College for financial support of this work, G. Yuan and Y. Lin for helpful discussions, and a Rodin fellowship (to S.Z.).

REFERENCES AND NOTES

1. Tarascon, J. M.; Armand, M. Issues and Challenges Facing Rechargeable Lithium Batteries. *Nature* **2001**, *414*, 359–367.
2. Kasavajjula, U.; Wang, C.; Appleby, A. J. Nano- and Bulk-Silicon-Based Insertion Anodes for Lithium-Ion Secondary Cells. *J. Power Sources* **2007**, *163*, 1003–1039.
3. Arico, A. S.; Bruce, P.; Scrosati, B.; Tarascon, J. M.; Van Schalkwijk, W. Nanostructured Materials for Advanced Energy Conversion and Storage Devices. *Nat. Mater.* **2005**, *4*, 366–377.
4. Graetz, J.; Ahn, C. C.; Yazami, R.; Fultz, B. Highly Reversible Lithium Storage in Nanostructured Silicon, Electrochem. *Solid State Lett.* **2003**, *6*, A194–A197.

5. Chan, C. K.; Peng, H.; Liu, G.; McIlwrath, K.; Zhang, X. F.; Huggins, R. A.; Cui, Y. High-Performance Lithium Battery Anodes Using Silicon Nanowires. *Nat. Nanotechnol.* **2008**, *3*, 31–35.
6. Wang, Y.; Takahashi, K.; Shang, H.; Cao, G. Synthesis and Electrochemical Properties of Vanadium Pentoxide Nanotube Arrays. *J. Phys. Chem. B* **2005**, *109*, 3085–3088.
7. Mosby, J. M.; Prieto, A. L. Direct Electrodeposition of Cu_2Sb for Lithium-Ion Battery Anodes. *J. Am. Chem. Soc.* **2008**, *130*, 10656–10661.
8. Johnson, D. C.; Mosby, J. M.; Riha, S. C.; Prieto, A. L. Synthesis of Copper Silicide Nanocrystallites Embedded in Silicon Nanowires for Enhanced Transport Properties. *J. Mater. Chem.* **2010**, *20*, 1993–1998.
9. Wang, G. X.; Ahn, J. H.; Yao, J.; Bewlay, S.; Liu, H. K. Nanostructured Si-C Composite Anodes for Lithium-Ion Batteries. *Electrochem. Commun.* **2004**, *6*, 689–692.
10. Song, T.; Xia, J.; Lee, J.-H.; Lee, D. H.; Kwon, M.-S.; Choi, J.-M.; Wu, J.; Doo, S. K.; Chang, H.; Park, W. I.; *et al*. Arrays of Sealed Silicon Nanotubes as Anodes for Lithium Ion Batteries. *Nano Lett.* **2010**, *10*, 1710–1716.
11. Li, Y.; Tan, B.; Wu, Y. Mesoporous Co_3O_4 Nanowire Arrays for Lithium Ion Batteries with High Capacity and Rate Capability. *Nano Lett.* **2008**, *8*, 265–270.
12. Wang, D. H.; Choi, D. W.; Li, J.; Yang, Z. G.; Nie, Z. M.; Kou, R.; Hu, D. H.; Wang, C. M.; Saraf, L. V.; Zhang, J. G.; et al. Self-Assembled TiO_2-Graphene Hybrid Nanostructures for Enhanced Li-Ion Insertion. *ACS Nano.* **2009**, *3*, 907–914.
13. Meethong, N.; Huang, H. Y. S.; Speakman, S. A.; Carter, W. C.; Chiang, Y. M. Strain Accommodation During Phase Transformations in Olivine-Based Cathodes as a Materials Selection Criterion for High-Power Rechargeable Batteries. *Adv. Funct. Mater.* **2007**, *17*, 1115–1123.
14. Kang, B.; Ceder, G. Battery Materials for Ultrafast Charging and Discharging. *Nature* **2009**, *458*, 190–193.
15. Dong, W.; Rolison, D. R.; Dunna, B. Electrochemical Properties of High Surface Area Vanadium Oxide Aerogels. *Electrochem. Solid-State Lett.* **2000**, *3*, 457–459.
16. Santos-Peña, J.; Brousse, T.; Schleich, D. Mg_2Si and MSi_2 (M = Ca, Fe) Silicon Alloys as Possible Anodes for Lithium Batteries. *Ionics* **2000**, *6*, 133–138.
17. Netz, A.; Huggins, R.; Weppner, W. Investigations of a Number of Alternative Negative Electrode Materials for Use in Lithium Cells. *Ionics* **2001**, *7*, 433–439.
18. Lee, H.-Y.; Lee, S.-M. Graphite-FeSi Alloy Composites as Anode Materials for Rechargeable Lithium Batteries. *J. Power Sources* **2002**, *112*, 649–654.
19. Kim, I.-C.; Byun, D.; Lee, S.; Lee, J. K. Electrochemical Characteristics of Copper Silicide-Coated Graphite as an Anode Material of Lithium Secondary Batteries. *Electrochim. Acta* **2006**, *52*, 1532–1537.
20. Lee, Y. S.; Lee, J. H.; Kim, Y. W.; Sun, Y. K.; Lee, S. M. Rapidly Solidified Ti-Si Alloys/Carbon Composites as Anode for Li-Ion Batteries. *Electrochim. Acta* **2006**, *52*, 1523–1526.
21. Liu, W.-R.; Wu, N.-L.; Shieh, D.-T.; Wu, H.-C.; Yang, M.-H.; Korepp, C.; Besenhard, J. O.; Winter, M. Synthesis and Characterization of Nanoporous NiSi−Si Composite Anode for Lithium-Ion Batteries. *J. Electrochem. Soc.* **2007**, *154*, A97–A102.
22. Yan, J. M.; Huang, H. Z.; Zhang, J.; Yang, Y. The Study of Mg_2Si/Carbon Composites as Anode Materials for Lithium Ion Batteries. *J. Power Sources* **2008**, *175*, 547–552.
23. Hwang, C.-M.; Lim, C.-H.; Yang, J.-H.; Park, J.-W. Electrochemical Properties of Negative Simox Electrodes Deposited on a Roughened Substrate for Rechargeable Lithium Batteries. *J. Power Sources* **2009**, *194*, 1061–1067.
24. Zhou, S.; Liu, X. H.; Lin, Y. J.; Wang, D. W. Spontaneous Growth of Highly Conductive Two-Dimensional $TiSi_2$ Nanonets. *Angew. Chem., Int. Ed.* **2008**, *47*, 7681–7684.
25. Zhou, S.; Liu, X.; Lin, Y.; Wang, D. Rational Synthesis and Structural Characterizations of Complex $TiSi_2$ Nanostructures. *Chem. Mater.* **2009**, *21*, 1023–1027.
26. Zhou, S.; Liu, X. H.; Wang, D. W. Si/$TiSi_2$ Heteronanostructures as High Capacity Anode Material for Li Ion Batteries. *Nano Lett.* **2010**, *10*, 860–863.
27. Wang, T.; Oh, S.-Y.; Lee, W.-J.; Kim, Y.-J.; Lee, H.-D. *Ab Initio* Comparative Study of C54 and C49 $TiSi_2$ Surfaces. *Appl. Surf. Sci.* **2006**, *252*, 4943–4950.
28. Levi, M. D.; Aurbach, D. Simultaneous Measurements and Modeling of the Electrochemical Impedance and the Cyclic Voltammetric Characteristics of Graphite Electrodes Doped with Lithium. *J. Phys. Chem. B* **1997**, *101*, 4630–4640.
29. Levi, M. D.; Lu, Z.; Aurbach, D. Application of Finite-Diffusion Models for the Interpretation of Chronoamperometric and Electrochemical Impedance Responses of Thin Lithium Insertion V_2O_5 Electrodes. *Solid State Ionics.* **2001**, *143*, 309–318.
30. Ryu, J. H.; Kim, J. W.; Sung, Y. E.; Oh, S. M. Failure Modes of Silicon Powder Negative Electrode in Lithium Secondary Batteries, Electrochem. *Solid State Lett.* **2004**, *7*, A306–A309.
31. Liu, W.-R.; Wang, J.-H.; Wu, H.-C.; Shieh, D.-T.; Yang, M.-H.; Wu, N.-L. Electrochemical Characterizations on Si and C-Coated Si Particle Electrodes for Lithium-Ion Batteries. *J. Electrochem. Soc.* **2005**, *152*, A1719–A1725.
32. Zhang, Y.; Zhang, X. G.; Zhang, H. L.; Zhao, Z. G.; Li, F.; Liu, C.; Cheng, H. M. Composite Anode Material of Silicon/Graphite/Carbon Nanotubes for Li-Ion Batteries. *Electrochim. Acta* **2006**, *51*, 4994–5000.
33. Jiang, T.; Zhang, S.; Qiu, X.; Zhu, W.; Chen, L. Preparation and Characterization of Silicon-Based Three-Dimensional Cellular Anode for Lithium Ion Battery. *Electrochem. Commun.* **2007**, *9*, 930–934.
34. Moss, P. L.; Au, G.; Plichta, E. J.; Zheng, J. P. An Electrical Circuit for Modeling the Dynamic Response of Li-Ion Polymer Batteries. *J. Electrochem. Soc.* **2008**, *155*, A986–A994.
35. Chan, C. K.; Ruffo, R.; Hong, S. S.; Cui, Y. Surface Chemistry and Morphology of the Solid Electrolyte Interphase on Silicon Nanowire Lithium-Ion Battery Anodes. *J. Power Sources* **2009**, *189*, 1132–1140.
36. Ruffo, R.; Hong, S. S.; Chan, C. K.; Huggins, R. A.; Cui, Y. Impedance Analysis of Silicon Nanowire Lithium Ion Battery Anodes. *J. Phys. Chem. C* **2009**, *113*, 11390–11398.
37. Thompson, A. H. Electrochemical Potential Spectroscopy: A New Electrochemical Measurement. *J. Electrochem. Soc.* **1979**, *126*, 608–616.